Chemosphere 221 (2019) 11–20

Contents lists available at ScienceDirect

Chemosphere

journal homepage: www.elsevier.com/locate/chemosphere

Cell surface characterization and trace metal adsorptive properties of anaerobic ammonium-oxidizing (anammox) consortia

Yuxia Liu [a, b], Wei Xu [c], Lei Bao [d], Yanwei Li [d], Sitong Liu [e], Qingzhu Zhang [d], Daniel S. Alessi [f], Kurt O. Konhauser [f, *], Huazhang Zhao [b, **]

[a] State Key Laboratory of Petroleum Pollution Control, Beijing Key Lab of Oil & Gas Pollution Control, China University of Petroleum-Beijing, Beijing 10249, China
[b] Key Lab of Water & Sediment Sciences (Ministry of Education), College of Environmental Science & Engineering, Peking University, Beijing 100871, China
[c] Beijing Engineering Research Center for Advanced Wastewater Treatment, College of Environmental Science & Engineering, Peking University, Beijing 100871, China
[d] Environmental Research Institute, Shandong University, Jinan 250100, China
[e] State Key Lab Plateau Ecology & Agriculture, Qinghai University, Xining 810016, China
[f] Department of Earth & Atmospheric Sciences, University of Alberta, Edmonton, Alberta, T6G 2E3, Canada

HIGHLIGHTS

- Anammox consortia surfaces primarily contain carboxyl, amine, and hydroxyl sites.
- Deprotonation of above functional sites lead to negative surface charge.
- Carboxyl and hydroxyl sites can form stable Cd complexes.
- Carboxyl and hydroxyl sites promote bacterial aggregation and solid-liquid separation.
- Anammox consortia have the potential to adsorb and detoxify metal cations.

ARTICLE INFO

Article history:
Received 4 July 2018
Received in revised form
19 December 2018
Accepted 3 January 2019
Available online 6 January 2019

Handling Editor: A. Adalberto Noyola

Keywords:
Anammox
Acid-base titration
Adsorption
Cd
SCM
DFT

ABSTRACT

Interactions between metals and anaerobic ammonium oxidizing consortia substantially affect the quality of wastewater treatment plant effluent. In this study, we conducted acid-base titrations to ascertain the surface reactivity and proton adsorptive capacity of anammox consortia. A combination of titration data modeling and infrared spectroscopy suggested the presence of carboxyl, amine, and hydroxyl groups. Cd adsorption experiments demonstrate that 1 g of dry biomass could bind an equivalent of 7.12×10^{-6} mol/L of Cd. Density functional theory calculations further reveal that carboxyl and hydroxyl groups are able to form stable Cd complexes. Furthermore, considerable carboxyl and hydroxyl groups promote bacterial aggregation, and thus solid-liquid separation. The results of this study highlight the potential role of anammox consortia in adsorbing metal cations, and thus help to improve the understanding of the universally significant contribution of anammox consortia at the detoxification of metal cations in wastewater treatment systems.

1. Introduction

Anaerobic ammonium-oxidizing (Anammox) bacteria utilize ammonium (NH_4^+) as an electron donor and nitrite (NO_2^-) as an electron acceptor. This reaction forms nitrogen gas (N_2) anaerobically in the absence of a carbon source and without N_2O production (Strous et al., 1998; Zhang et al., 2015a).

$$NH_4^+ + NO_2^- \rightarrow N_2 + 2H_2O \quad (1)$$

Anammox bacteria are demonstrated to be ubiquitous in various natural ecosystems, including marine environments, estuarine

* Corresponding author.
** Corresponding author.
E-mail addresses: kurtk@ualberta.ca (K.O. Konhauser), zhaohuazhang@pku.edu.cn (H. Zhao).

https://doi.org/10.1016/j.chemosphere.2019.01.025
0045-6535/

sediments, freshwater and terrestrial environments (Kuypers et al., 2003; Rich et al., 2008; Jaeschke et al., 2009; Li et al., 2010). Anammox bacteria were recently discovered to be important in the oceanic nitrogen cycle (generating 10%–65% of N_2 production) based on the widespread occurrence of ammonium consumption in suboxic marine settings (Kuypers et al., 2003; Rich et al., 2008). As a result, an anammox cell density of approximately 1900 ± 800 cells/mL would be needed to account for the observed ammonium oxidation rates in the suboxic zone (Kuypers et al., 2003).

The anammox process has remarkable potential for treating ammonia-rich wastewater because there is no requirement for aeration or an exogenous electron donor, low sludge production, high nitrogen removal rates, and a potential reduction in the emission of greenhouse gases versus current wastewater treatment plant technologies (Zhang et al., 2015b). The anammox process was first documented in wastewater bioreactors (Mulder et al., 1995; Rich et al., 2008). Over the past decade many technologies have been developed to improve the applicability of the anammox process to nitrogen rich wastewater (Chen et al., 2009; Li et al., 2010). According to available data, over 100 full-scale annamox-based process plants have been installed worldwide (Lackner et al., 2014; Zhang et al., 2015a).

Certain streams often contain high concentrations of heavy metals (e.g., Cu, Zn, Cd, Pb and Ni), especially those draining municipal landfill leachates, anaerobically digested piggery/dairy slurries, metal refineries, industry producing nitrogenous fertilizers, and semiconductor manufacturers (Lotti et al., 2012; Zhang et al., 2016b). Heavy metals in landfill leachates are reported to be in the range of several hundreds of μg/L (Baun and Christensen, 2004). For instances, the concentration of Cu in semiconductor effluents were 5–100 mg/L, and the Zn levels in raw swine wastewater and landfill leachates were 1.5–30 mg/L and 0.05–1000 mg/L, respectively (Zhang et al., 2015b, 2016b). The concentration of Cd in sewage sludge collected from municipal and industrial wastewater treatment plants can range from 0.90 to 112.03 mg/kg (dry weight) (Wang et al., 2005).

When applying anammox bacteria to high-concentration nitrogen streams with elevated concentrations of heavy metals, the reactivity and growth of anammox bacteria may be inhibited. As a result, the nitrogen removal efficiency may be adversely affected. For example, the 50% inhibitory concentration of nitrogen removal rate by anammox bacteria for Cd, Cu, and Zn were reported to be 11.16, 6.5 and 12.5 mg/L, respectively (Bi et al., 2014; Kimura and Isaka, 2014). In the past decade, the database pertaining to the potential inhibitory impact of heavy metals on the performance of the anammox bacterial activity has received much attention. Yet to our knowledge, few studies have examined anammox bacterial surface reactivity and its role in metal complexation. Anammox cells have both an inner and an outer membrane, and a putative S-layer (Egli et al., 2001). Previous studies revealed that anammox bacterial cell surfaces contain a variety of reactive ligands, such as carboxyl, hydroxyl, and amine groups resulting from proteins, carbohydrates, and polysaccharide moieties (Bi et al., 2014; Hou et al., 2015; Zhang et al., 2016a). These ligands are capable of binding metal cations from solutions, thus causing metal species transport and bacterial aggregation due to complexation and bridging (Kumar et al., 2004).

The purpose of this study was to describe the surface charge properties, protonation behavior, and metal adsorption capacity of anammox consortia. Cd(II) was chosen to compare the metal sorption ability of anammox consortia with other bacterial species, including microaerophilic Fe(II)-oxidizers (e.g., Martinez et al., 2016) and cyanobacteria (e.g., Liu et al., 2015), with different metabolisms and cell surface structures. We had three objectives: to (1) constrain the acid dissociation constants (pKa values) and concentrations of proton-active sites that may bind metals to the cell surface of anammox consortia, using acid-base titrations and SCM modeling; (2) determine anammox consortia efficiency toward Cd(II) removal from solution by quantifying the adsorption affinities of Cd(II) at various metal:bacterial site concentrations as a function of pH; and (3) explore the structural geometry of the Cd complexes and to determine the most stable Cd complex structures by density functional theory (DFT) calculations.

2. Materials and methods

2.1. Bacterial growth

The anammox consortia studied in these experiments were cultivated and maintained in a laboratory-scale (2 L) sequencing batch reactor (SBR). The consortia were dominated by anammox bacteria of the genus *Candidatus Brocadia fulgida* (Hou et al., 2015). The anammox cells appeared as red particle aggregates, as was shown in Fig. S1. The synthetic wastewater feed for the anammox consortia was prepared with tap water including $(NH_4)_2SO_4$ (0.2357 g/L), $NaNO_2$ (0.2465 g/L), $NaHCO_3$ (0.5 g/L), KH_2PO_4 (0.025 g/L), $CaCl_2{\cdot}2H_2O$ (0.01 g/L), $MgSO_4$ (0.1 g), $FeSO_4{\cdot}7H_2O$ (0.005–0.01 g/L), EDTA·2Na (0.006 g/L) and trace element solutions (van de Graaf et al., 1996; Zhang et al., 2016a). The composition of the trace element solutions has been described in a previous study (van de Graaf et al., 1996). pH and temperature of the reactors were controlled at 7.4–8.3 and 35 ± 0.5 °C, respectively. Anaerobic conditions were maintained by flushing nitrogen gas throughout the period of reactor operation. The stirring speed of the reactor was set at 140 rpm to improve mass transfer. The influent and effluent were taken every 2–3 days for the measurements of ammonium, nitrite, nitrate, 5-min and 30-min sludge volume indices (SVI5 and SVI30), total suspended solids (TSS) and volatile suspended solids (VSS) concentrations according to standard colorimetric methods (APHA, 1998), with the aim to evaluate the growth of anammox consortia. When the change multiple of biomass yield, the anammox consortia was thought to grow to exponential phase. Then the anammox consortia was harvested by centrifugation at room temperature for following experiments.

2.2. Scanning electron microscopy (SEM)

For SEM imaging, anammox consortia were first washed 3 times in 0.1 M phosphate buffer saline (PBS, pH 7.2) and then fixed in 2.5% gluteraldehyde − 2% paraformaldehyde at 4 °C overnight. After fixation, the samples were dehydrated through a graded ethanol series (15 min in each 50%, 85%, and 100% ethanol solution) and then dried in a desiccation chamber overnight. Samples were then placed on 1 × 1 cm microscope slide and imaged on a Philips FEI XL 30 Scanning Electron Microscope operating at 20 kV.

2.3. Fourier transform infrared (FTIR) spectroscopy

FTIR spectroscopy was conducted to characterize the major functional groups of organic compounds exposed on the anammox consortia cell envelopes. Immediately after harvesting, cells were washed three times in 0.01 M NaCl electrolyte solutions and then oven dried at 60 °C for 24 h. KBr pellets containing 0.20% (dry weight) of the sample were prepared, and then examined on a Deuterated Tri Glycine Sulfate (DTGS) detector attached to a Thermo Nicolet is50 FTIR Spectrometer. Infrared spectra were produced by averaging 256 scans over the wavenumber range between 4000 and 500 cm^{-1} at a resolution of 4 cm^{-1}, and in absorbance mode. During data processing spectra were corrected for a KBr background. Measurements were carried out in duplicate using

two biological replicates. In order to compare the Cd-free and Cd-loaded spectrum collected on our study, all spectra were baseline corrected and area normalized according to Felten et al. (2015).

2.4. Zeta potential measurements

Zeta potential measurements were conducted to assess the net surface charge characteristics of anammox consortia (without ESP extraction). To do so, the cells were harvested, washed, and dissolved in 10 mL 0.01 M NaCl solution to a concentration of approximately 0.1 g volatile suspended solid (VSS) per liter. The solution pH was adjusted in the range of 3–10 by adding small aliquots of HCl (0.016, 0.16, and 1.6 M) or NaOH (0.019, 0.19, and 1.9 M) and stirring until the pH stabilized. A Zetasizer Nano ZS instrument (Malvern. Inc., USA) was used to measure the zeta potential at 25 °C. Data were obtained by the calculation of an average of 10 readings for 3 biological replicates. Matching cell-free NaCl solutions were used as controls.

2.5. Acid-base titrations and modeling

In order to conduct acid-base titrations, anammox consortia were harvested from the growth solutions by centrifugation, transferred to centrifuge tubes, and washed five times in 0.01 M NaCl (the same electrolyte used in the experiments). During each wash, the cells were suspended in fresh electrolyte solution using a vortex machine. Bacteria were centrifuged for 10 min at 10,000 g to form a pellet at the base of the centrifuge tube and the electrolyte was discarded. After the final wash, the biomass was re-suspended in approximately 50 mL of electrolyte solution (exactly weighed) in a titration flask. The flask was fitted with a double-junction glass pH electrode (Orion ROSS ultra, filled with 3 M KCl) which was calibrated using commercial pH buffers, as well as a magnetic stir bar, titrant dispenser, and Nitrogen (N_2) gas line. The suspension was acidified to pH 3.0 with 2 M HCl, sealed with Parafilm, and purged with N_2 for 30 min prior to, and throughout titrations, to maintain a CO_2-free atmosphere in the flask.

Titrations were performed alkalimetrically from pH 3.0 to 11.0 using a KEM AT-500N autotitrator that variably delivered CO_2-free 0.01 M NaOH as described by Liu et al. (2015). The incremental volume of base added, and corresponding pH changes, were recorded for each titration step. Each addition of base occurred only after a pH electrode stability of 0.1 mV/s was attained, for a typical total titration time of approximately 50 min. Titrations were carried out a minimum of three times using separate batches of bacterial cultures. Blank titrations were performed for machine calibration, using bacteria-free 0.01 M NaCl solutions. Once pH 11 was reached, reverse 'down-pH' titrations were performed, decreasing the suspension pH to 3 with aliquots of 0.01 M HCl in order to assess possible hysteresis in the titration curves, a test to ensure the reversibility of the titration process. Immediately following titration, biomass was filtered onto preweighed Whatman GF/C #42 filters (0.45 μm) and oven dried at 65 °C for 48 h for dry weight determination.

For each titration step, the charge balance can be calculated and written as following:

$$[C_a - C_b] = [-Q] + \left[H^+\right] - \left[OH^-\right] \quad (2)$$

Where [C_a - C_b] is the concentration of acid added minus the concentration of base added; [H^+] and [OH^-] are the concentrations of proton and hydroxyl ions, respectively, and [-Q] is the negative charge excess owing to deprotonation of bacterial ligands in solution, normalized to per gram of biomass.

A non-electrostatic surface complexation model was used to fit titration data to determine the acidity constants and site concentrations of functional groups on anammox consortia. The deprotonation of a functional group can be represented by the following generic reaction:

$$R - L_nH^0 \leftrightarrow R - L_n^- + H^+ \quad (3)$$

The acidity constants, K_a, for reaction (2) can be defined as:

$$K_a = \frac{\left[R - L_n^-\right] \cdot a_{H^+}}{\left[R - L_nH^0\right]} \quad (4)$$

Where R is the bacterium to which the functional group type L was attached, $[R - L_n^-]$ and $[R - L_nH^0]$ represents the concentration of deprotonated and protonated sites, respectively, and a_{H^+} represents the activity of protons in bulk solution.

The least square fitting program FITEQL 4.0 (Herbelin and Westall, 1999) was used to model the acid-base titration data and solve for a predetermined number of surface sites, the site acidity constants (expressed as pKa, equivalent to −log K_a) and corresponding site concentrations that best describe the excess charge data. In this case, a three-site model provided the best fit, with V(Y) values in the range of $0.1 < V(Y) < 20$ (Westall, 1982).

2.6. Cadmium adsorption experiments and modeling

To determine the removal of aqueous Cd(II) that occurred upon exposure to washed anammox consortia, 10 g/L of the bacterial biomass was suspended in a 0.01 M NaCl electrolyte solutions. Three Cd(II) concentrations (8.9×10^{-6} M, 8.9×10^{-5} M and 2.2×10^{-4} M) were tested for Cd(II) adsorption. After an initial 10 min equilibration time, 10 mL aliquots were transferred to polypropylene centrifuge tubes and adjusted to starting pH values between pH 3 and 9, in 1 pH unit intervals, using HCl (0.016, 0.16 and 1.6 M) or NaOH (0.019, 0.19 and 1.9 M). The systems were mixed via end-over-end rotation at 140 rpm for 24 h to allow time for equilibration between the Cd(II) and the cells, after which the final (equilibrium) pH of each vessel was measured. The individual vessels were then centrifuged at 10,000 g and the resulting supernatant filtered through a 0.22 μm nylon membrane. The filtered supernatants were analyzed for Cd(II) concentrations using an Inductively Coupled Plasma-Optical Emission Spectrometer (ICP-OES), calibrated with matrix-matched standards (Thermo Fisher Scientific). The concentration of Cd(II) adsorbed to the cells in each vessel was calculated by subtracting the concentration of Cd(II) that remained in solution (supernatant) from the original Cd(II) solution concentrations. Control experiments were conducted without bacteria to determine if Cd(II) was lost to the experimental apparatus or by precipitation in the timeframe of the adsorption experiments.

The reversibility of Cd(II) adsorption behavior was also tested in our experiments, following the methods of Liu et al. (2015). The Cd-loaded cells at 8.9×10^{-6} M, 8.9×10^{-5} M and 2.2×10^{-4} M Cd(II) concentration, in the presence of the 0.01 M NaCl ionic strength electrolyte, were harvested, rinsed and re-suspended in 0.01 M NaCl solutions. The pH of the suspensions was adjusted to 3.0 by using 2 M HCl in order to desorb surface-bound Cd(II) from cells. After being gently agitated for 24 h, the suspensions were centrifuged and filtered as previously described, and the Cd(II) concentration in the supernatant was measured. The amount of Cd(II) measured was compared to the concentration of Cd(II) adsorbed to calculate the percent of Cd(II) recovered.

Experimental Cd(II) adsorption data were assessed by fitting

experimental metal sorption data with FITEQL, using the non-electrostatic complexation modeling approach, using the average site concentrations of anammox consortia and their acidity constants calculated from acid-base titrations, as described above. In the model, six aqueous cadmium hydrolysis reactions, three cadmium carbonate complexes, as well as aqueous cadmium chloride complexes were considered (Table S1; Zirino and Yamamoto, 1972; Baes and Mesmer, 1976; Stipp et al., 1993). Cd(II) concentrations adsorbed onto anammox consortia were determined based on the following hypothesized surface adsorption reactions:

$$R - L_n^- + Cd^{2+} \rightarrow R - L_nCd^+ \quad (5)$$

Cd-ligand stability constants were defined as:

$$K_{CdL} = \frac{[R - L_nCd^+]}{[R - L_n^-] \cdot a_{Cd^{2+}}} \quad (6)$$

Where $[R - L_nCd^+]$ was the concentration of the Cd-ligand organic complex, $[R - L_n^-]$ was the concentration of ligands and $a_{Cd^{2+}}$ was the activity of Cd^{2+} in solution. The equilibrium constant, K_{CdL} was reported as log K_{CdL}.

2.7. DFT calculations

The geometries of D-glucuronic acid, L-fucose, D-glucosamine, D-glucose, Valine, Glutamic acid, Leucine, Alanine, Aspartic acid, as well as their binding complexes with Cd(II) were all optimized with the M06-2X method (Zhao and Truhlar, 2008) and basis set def2-SVP. The SMD solvation model was applied during geometry optimizations to represent water solvents (Marenich et al., 2009). All the calculations were performed with Gaussian 09 software (Frisch et al., 2013).

3. Results

3.1. Composition of the anammox consortia

SEM imaging (Fig. 1) of anammox consortia revealed that pair-cocci cells are of 1.5–3 μm in diameter. The bacteria cells were encapsulated and connected by extracellular polymeric substances (EPS) to form larger particles, which also apparently holding the cells tightly together.

In order to account for the functional groups present in the anammox consortia, FTIR analyses were performed (Fig. 2 and Table 1). Duplicate spectra from an individual culture were identical, so a representative spectrum was shown in Fig. 2. The peak assignments were as follows. Strong absorption peaks at 3000-2800 cm^{-1} were assigned to asymmetric stretching vibration of $-CH_3$ (2990 ± 5 cm^{-1} and 2950 ± 5 cm^{-1}), which were attributed to the fatty acid components found in membrane phospholipids (Schmitt and Flemming, 1998). The band at 1726 cm^{-1} was associated with the C═O and C−OH stretching vibrations of protonated carboxylic acid groups (Jiang et al., 2004). The amide I band at 1610 cm^{-1} and 1650 cm^{-1} were mainly assigned to C═O and C═C stretching associated with proteins (Yuan et al., 2011; Hou et al., 2015). The small band at 1238 cm^{-1} was representative amide III band, which was attributed to C−N stretching vibration in proteins (Yuan et al., 2011). The band at around 1434 cm^{-1} was attributed to the symmetric stretching of C═O in COO^- (Hou et al., 2015). Strong absorption peaks at 1387 cm^{-1} and 1325 cm^{-1} were tentatively assigned to symmetric deformation vibration of $-CH_3$ and wagging

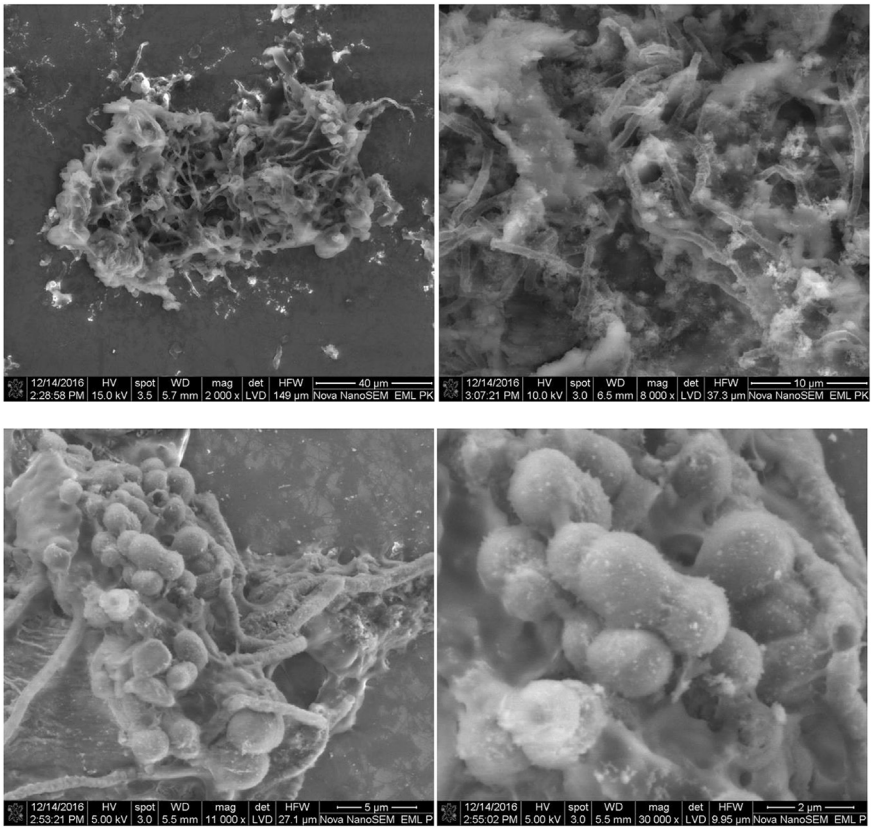

Fig. 1. SEM images of anammox consortia. (a) Full-profile of the consortia; (b) surface of the consortia; (c, d) interior of the consortia.

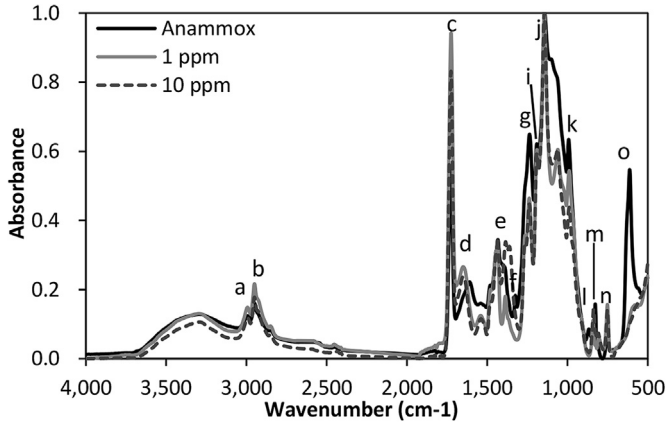

Fig. 2. FTIR absorbance spectra of anammox consortia at late exponential growth phase before and after exposure to solutions with Cd at pH 8.0.

Table 1
Summary of proposed functional groups and corresponding infrared wavelengths.

IR band	Wavelength (cm^{-1})	Functional groups assignment
a, b	3000–2800	ν_{as} of $-CH_3$ (Schmitt and Flemming, 1998)
c	1726	ν_s C=O of protonated carboxylic acid groups
d	1610	Stretching of C=O in amide I, associated with proteins and δ O–H of water (Yuan et al., 2011; Hou et al., 2015)
e	1434	ν_s of C=O in COO^- (Hou et al., 2015)
f	1325	symmetric deformation vibration of $-CH_3$ and wagging vibration of $>CH_2$ (Wen and Xu, 2016; Zhang et al., 2016a)
g	1237	C–N stretching vibration in proteins (Yuan et al., 2011)
i	1191	ν_s C–OH, ν_s C–O from carbohydrates
j	1142	C–OH stretching vibration and C–*O*–C asymmetric stretching vibration (shown as C–O stretching vibration) in polysaccharides (Wen and Xu, 2016; Zhang et al., 2016a)
k, l, m, n, o	<1000	fingerprint region

ν_s = symmetric stretching; ν_{as} = asymmetric stretching; δ = bending.

vibration of $>CH_2$, respectively, which were attributed to the fatty acid components found in membrane phospholipids (Wen and Xu, 2016; Zhang et al., 2016a). Absorption peaks at 1150-1000 cm^{-1} might be assigned to C–OH stretching vibration and C–*O*–C asymmetric stretching vibration (shown as C–O stretching vibration) in polysaccharides. Absorption peaks at 1000-900 cm^{-1} might be assigned to C–*O*–H out-of-plane bending vibration of COOH (e.g., D-glucuronic acid) (Wen and Xu, 2016; Zhang et al., 2016a). FTIR spectra revealed the presence of many functional groups such as carboxyl, amine and hydroxyl on anammox consortia.

Exposure to Cd(II) resulted in a slight change in the FTIR spectra as compared to Cd-free samples. The peak at 1610 cm^{-1} shifted to 1650 cm^{-1} after loading Cd(II). Meanwhile, the peak at 1325 cm^{-1} shifted to 1387 cm^{-1} after Cd(II) loaded. Changes in the position of the band at 1610 cm^{-1} and 1325 cm^{-1} indicate that carboxyl and hydroxyl groups were responsible for the binding of Cd(II) because both of these biopolymers contains numerous carboxyl and hydroxyl groups. In addition, Cd(II)-loaded cells exhibited small peaks at 1540 cm^{-1} and 1060 cm^{-1} were observed. Absorption peak at 1540 cm^{-1} correspond to the C–N–H bending vibration of amide II or symmetric deformation vibration of NH_3^+ in amino acids. While absorption peak at 1060 cm^{-1} might be assigned to C–OH stretching vibration and C–*O*–C asymmetric stretching vibration (shown as C–O stretching vibration) in polysaccharides (e.g., D-glucose, L-fucose, D-glucuronic acid, and D-glucosamine) (Jiang et al., 2004; Wang et al., 2012; Wen and Xu, 2016). Compared to Cd-free cells, the peaks disappeared within the range of 867 cm^{-1} and 613 cm^{-1} for Cd-loaded cells. Small peaks at 813 and 613 cm^{-1} might be related to $-NH_2$ twisting vibration and COO^- functional groups, which is easily affected by C–H wagging vibration and other charged atoms. In this regard, Cd atoms in the solutions might pose an effect on the COO^- and $-NH_2$ functional groups and lead to the disappearance of the corresponding peaks at 867 cm^{-1} and 613 cm^{-1} (Wen and Xu, 2016).

In summary, the FTIR results demonstrate the presence of carboxyl (–COOH), hydroxyl (–OH), and primary amine ($-NH_2$) groups in anammox consortia (Yuan et al., 2011), and that carboxyl, hydroxyl and amine groups might play an important role in the binding of Cd by anammox consortia.

3.2. Reactivity of the anammox consortia

Zeta potential measurements (Fig. 3) revealed that anammox consortia continuously exhibited a net negative surface charge over the pH 3–10, with values ranging from −1.2 to −35.7 mV. Specifically, anammox consortia displayed a sharp increase in electronegativity from pH 3 to 6, above which it remained constant. Within the pH range of 9–10, the electronegativity decreased sharply to −35.7 mV. The general zeta potential measurements illustrate that the surface of anammox consortia has much more electronegative functional groups than electropositive ones.

Table 2 and Fig. 4 present a summary of the pKa values and corresponding site densities (mmol/g dry weight) associated with bacterial cell surface of anammox consortia obtained from the modeling of acid-base titration data. According to the FTIR spectra, the first proton-active site (pKa_1) at pH 3.92 can be attributed to carboxyl groups, the second site (pKa_2) at pH 6.69 might be attributed to amine acids that exist in the form of bioorganic molecules such as proteins, and the third site (pKa_3) at pH 9.31 can be attributed to hydroxyl groups (Wang et al., 2012). For the three sites, the binding site densities were estimated to be 0.26 ± 0.08, 0.82 ± 0.05, and 2.75 ± 0.56 mmoL/g (dry weight), respectively (Fig. 4B). A summation of the ligand concentrations across the analyzed pH range revealed that anammox consortia exhibited an average total site densities of 3.83 ± 0.43 mmoL/g (dry weight) in the 0.01 M NaCl electrolyte.

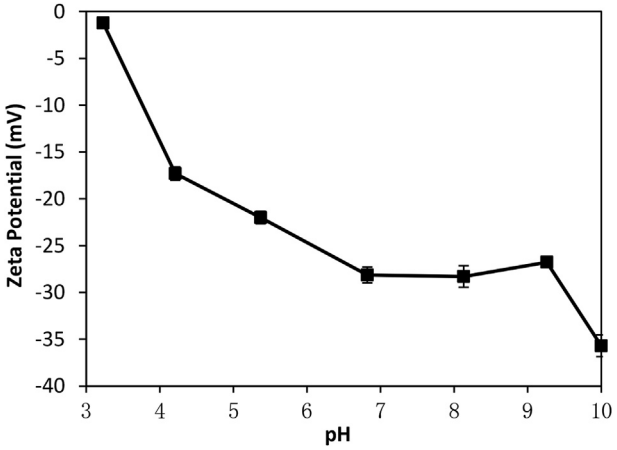

Fig. 3. Zeta potential measurements conducted using suspensions of anammox consortia incubated in 0.01 M NaCl buffer as a function of pH. The average of three independent experiments is plotted. Error bars represent the ±1-sigma standard deviation of the averaged data sets.

Table 2
Parameters obtained from best-fit, non-electrostatic proton adsorption models of titration data (pKa and total density of ligand) and best-fit Cd-ligand stability constants (-log KCdL) for anammox consortia.

Ligand class	Average pKa	Mean L_T (mmol g^{-1})	Functional groups	Log K_{CdL}		
				1 ppm	10 ppm	25 ppm
A	3.92 ± 0.05	0.26 ± 0.08	Carboxyl	1.22	1.46	1.39
B	6.69 ± 0.04	0.82 ± 0.05	Amine	2.97	3.77	4.40
C	9.31 ± 0.12	2.75 ± 0.56	Hydroxyl	5.43	5.00	5.45

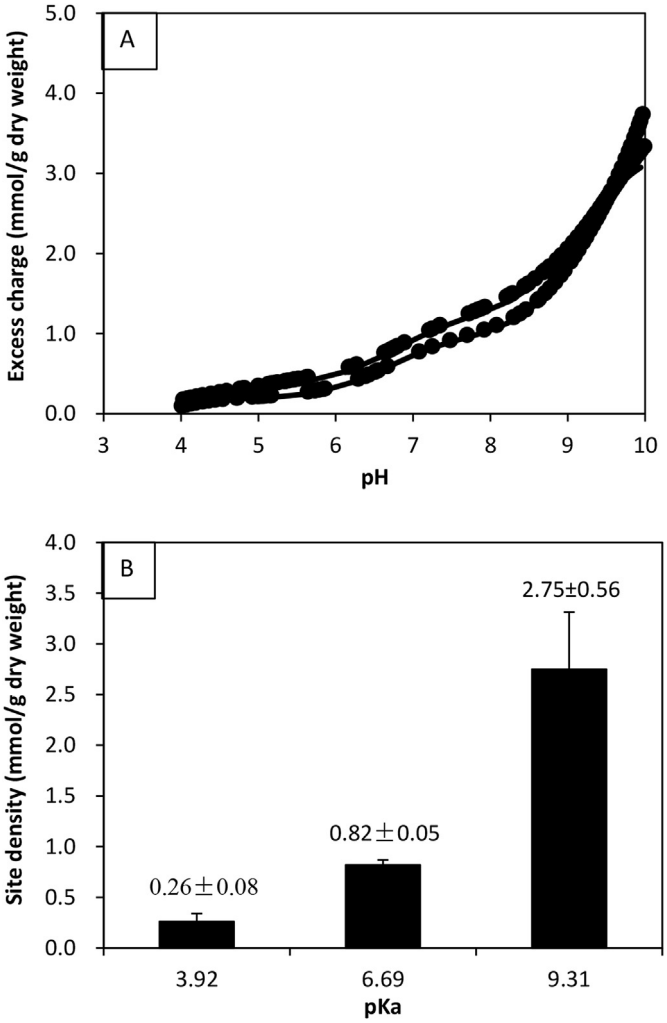

Fig. 4. (A) Potentiometric titration data for anammox consortia in terms of excess charge as a function of pH; ionic strength is 0.01 M NaCl. (B) Ligand densities of 3-pKa titration models at ionic strength of 0.01 M NaCl.

3.3. Cadmium adsorption to anammox consortia

Though Cd adsorption experiments were conducted between pH 3 and 9, only data within a pH range of 3.0–8.5 were considered. This is because preliminary speciation calculations, for a system containing 8.9×10^{-6} to 2.2×10^{-4} M Cd(II) in 0.01 M $NaNO_3$ or 0.56 M NaCl ionic strength solutions, indicates that precipitation of cadmium carbonate solids or $Cd(OH)_2$ (s) form at pH values greater than 8.5 (Liu et al., 2015). As shown in Fig. 5, there was a positive correlation between Cd(II) removed from solution and pH, and a negative correlation between Cd(II) removed and the initial concentration. In experiments with low Cd(II) concentrations (8.9×10^{-6} M, Fig. 5A), 50% removal of Cd(II) occurred at

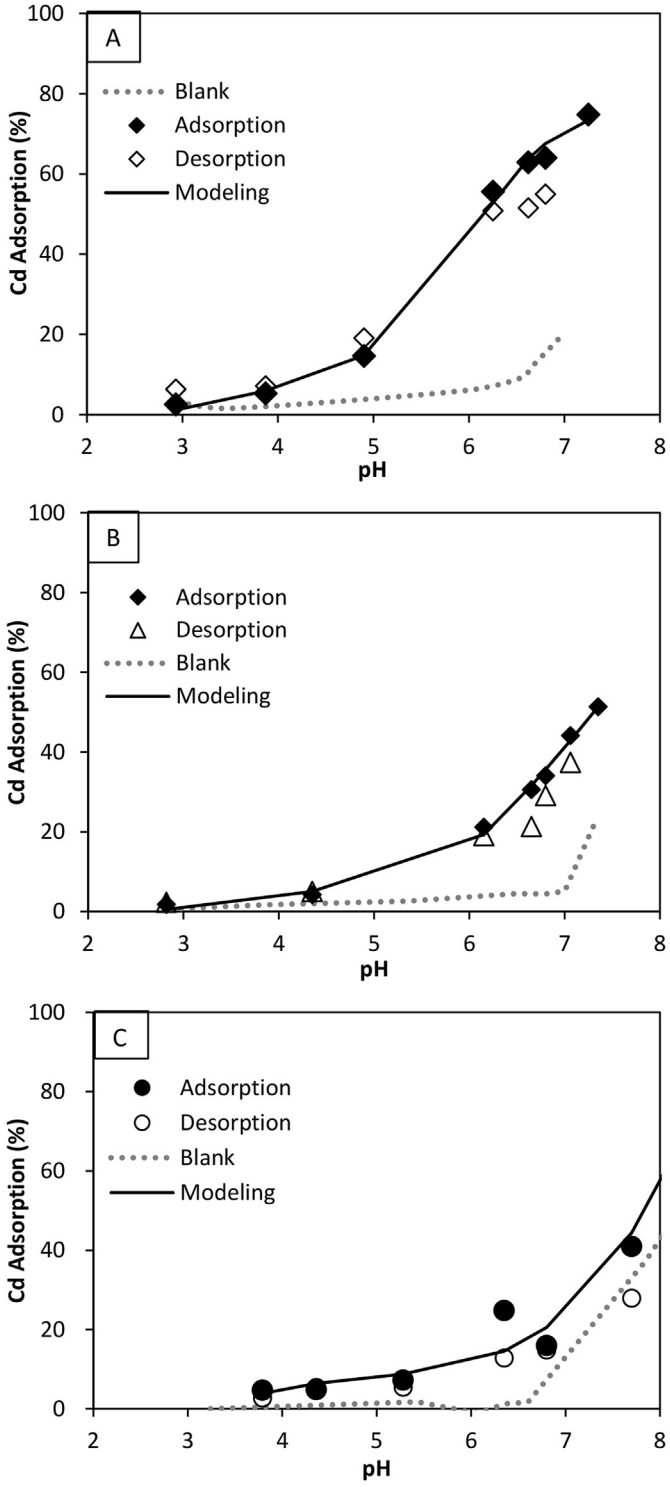

Fig. 5. Cd adsorption edges for anammox consortia exposed to 0.01 M NaCl ionic strength at three different Cd concentrations: (A) 8.9×10^{-6} M; (B) 8.9×10^{-5} M; (C) 2.2×10^{-4} M.

approximately pH 6.0, and nearly 80% of Cd(II) was removed at pH 7.5. At higher Cd(II) concentrations (8.9×10^{-5} M, Fig. 5B), the 50% Cd(II) uptake pH shifted to above pH 7.0, whereas at 2.2×10^{-4} M Cd(II), the point of 50% Cd(II) uptake occurred at approximately pH 8.0 (Fig. 5C). A decrease in Cd(II) removal from solution was observed when Cd(II) was gradually increased, suggesting that the functional groups were becoming saturated.

Reversibility of Cd(II) sorption to anammox consortia indicated that more than 85% of the adsorbed Cd(II) was desorbed from the anammox consortia. The missing recovery efficiency may be attributed to the loss of a limited amount of biomass during the adsorption/desorption cycle, or potentially, to an intracellular metal diffusion process (absorption). However, these cadmium desorption experiments confirmed that the primary mechanism of metal removal from solution was reversible cadmium adsorption to the anammox consortia.

As depicted in Table 2 and Fig. 5, Cd(II) adsorption behavior onto anammox consortia was fit using surface complexation models that invoke three distinct sites. For low Cd(II) concentrations (8.9×10^{-6} M), an excellent fit was achieved when carboxyl, amine and hydroxyl sites participated in Cd(II) adsorption (Fig. 5A); the Cd-ligand stability constants (as log K_{CdL}) determined for the three ligands were 1.22, 2.97 and 5.43, respectively. At higher initial Cd(II) concentrations (8.9×10^{-5} M), the Cd-ligand stability constants (as log K_{CdL}) determined for carboxyl, amine, and hydroxyl were 1.46, 3.77, and 5.00, respectively. At the highest Cd(II) concentration (2.2×10^{-4} M), the Cd-ligand stability constants (as log K_{CdL}) corresponding to carboxyl, amine, and hydroxyl sites were 1.39, 4.40, and 5.45, respectively. For all three metal concentrations, the Cd-ligand stability constants are remarkably close, which indicates that our SCM model is quite solid across the conditions tested.

3.4. Density functional theory (DFT) calculations

FTIR spectra of anammox consortia, proteins and polysaccharides indicate that −OH, −COOH, and $-NH_2$ groups were the key functional groups of the bacterial cell surface. Table S2 summarized 5 amino acids, i.e., Alanine (Ala), Leucine (Leu), Valine (Val), Aspartic (Asp) and Glutamic acid (Glu) and 4 monosaccharides, i.e., D-glucuronic acid, D-glucosamine, D-glucose, and L-Fucose as the main components of EPS associated with anammox consortia (Wang et al., 2013; Hou et al., 2015). Here, the structures of the 5 amino acids and 4 monosaccharides were optimized to describe their adsorption of Cd(II) on anammox consortia by means of DFT calculations (Fig. 6), and also to reveal which group(s) (i.e., −COOH, −OH, $-NH_2$) were mainly responsible for metal adsorption. Besides the −COOH, −OH, and $-NH_2$ functional groups noted above, the −COC functional group, which is abundant in monosaccharides, also has the potential to bind Cd(II). Our results showed that −OH and −COC functional groups were the principal functional groups of monosaccharides (~90%), while −COOH and $-NH_2$ were the main functional groups of amino acids (~90%).

The binding energies (E_{bd}) of Cd(II) with amino acids were generally higher than those with monosaccharides, indicating that Cd(II) ions prefer to bind with functional groups associated with proteins. For the monosaccharides, E_{bd} of Cd(II) with two −OH functional groups and one −OH and one −COC were 10.8–15.4 and 5.9–13.6 kcaL/mol, respectively. Thus, −OH was likely to play a more important role than −COC in the binding process. For the amino acids, E_{bd} of Cd(II) with −COOH and $-NH_2$ ranged from 18.2 to 20.7 kcaL/mol. Additionally, the −COOH in the R group of Asp can strongly bind with one Cd(II) cation through two interfacing −COOH bonds, with a corresponding E_{bd} of 26.2 kcaL/mol. Thus, −COOH likely plays a more important role than $-NH_2$ in the binding process.

Overall, computational results highlighted that (1) the −COC functional group played an important role in Cd(II) binding; (2) −OH was more important than −COC in the binding of Cd(II) with monosaccharides; and (3) −COOH was more important than $-NH_2$ in the binding of Cd(II) with amino acids.

4. Discussion

Using a combination of FTIR spectroscopic measurements and modeling of acid-base titration data, the anammox consortia contained carboxyl, amino, amine and hydroxyl groups in the pH range of 3–10. These functional groups become deprotonated with increasing pH, since the surface charge of bacterial cells, in general, is established by proton dissociation from surface exposed ligands (Fein et al., 2005). The net electronegativity of anammox consortia and a decrease in surface charge provides evidence that negatively charged carboxyl and hydroxyl groups occurred more frequently than positively charged amine sites. It is also clear that these ligands were highly reactive for binding metal cations under our experimental conditions.

The pKa values of surface functional groups associated on anammox consortia fall in the range, but are not exactly equivalent, to those pKa values of previous studies that use bacterial consortia or admixtures derived from a variety of environments (Table 3). This occurs because the magnitude of the dissociation constant is controlled by the structure of the molecule to which it is attached (Martell and Smith, 1977). Consequently, variable pKa values between anammox consortia and other bacterial consortia or mixtures suggest conformational variations within the wall macromolecules. Furthermore, titration experiments are only able to resolve those functional groups that contribute significant amounts of protons to solution. Minor groups are simply undetectable with the resolution of current techniques (Konhauser, 2007). Therefore, the model-derived binding sites do not cover and represent the entire suite of proton-active functional groups at the cell surface.

With regards to the average total site concentrations (the sum of the average concentrations of binding sites for each of the three surface sites), our anammox consortia have comparable binding site concentrations (dry weight) as reported for natural consortia or bacterial mixtures (Table 3). The variability represented in the consortia or mixtures is likely due to differences in bacterial growth conditions, growth media and titration procedures amongst the different studies (Borrok et al., 2004a, b; Laurent et al., 2009).

Collectively, our results show that anammox consortia display an overall net negative charge under the studied pH range. The adsorption of Cd(II) on anammox consortia significantly decreases with increasing Cd(II) concentration due to a higher loading of Cd(II) on surface functional groups. For instance, in the case of relatively high biomass:metal ratios (i.e., 8.9×10^{-6} M Cd experiments in 0.01 M electrolyte solutions), we determined that 1.0 g dry biomass of anammox consortia (containing 3.83 ± 0.43 mmol/g dry mass of deprotonated ligands) can bind an equivalent of 7.12×10^{-6} M of Cd(II) (pH = 8). This result was a magnitude lower than those bacterial consortia or mixtures grown either in nature or industrial contaminated sites (Table 3), but a magnitude higher than anaerobic photoferrotroph *Rhodovulum iodosum* (Martinez et al., 2016).

Due to the availability of proton-active functional groups on the cell surface, our data indicate that anammox consortia have the potential to play an important role in metal cycling – via adsorption – in wastewater treatment bioreactors. Given that average anammox consortia contain 42.0–57.7 g/L in an upflow anaerobic sludge bed (UASB) (Tang et al., 2011), a simple extrapolation suggests that a UASB bioreactor could potentially bind 2.1-2.9 $\times 10^{-5}$ M (wet: dry

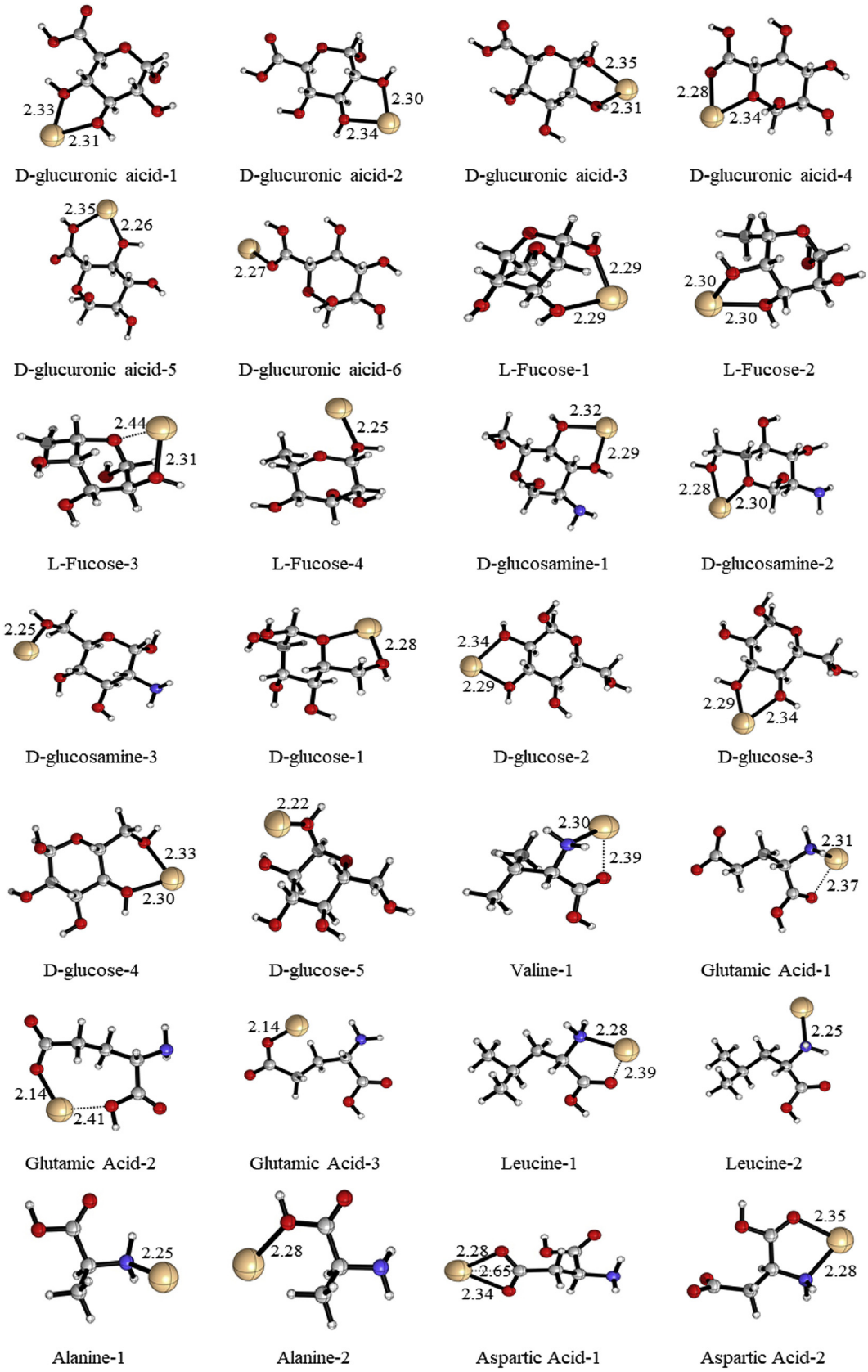

Fig. 6. The possible bonding sites of adsorption of cadmium by polysaccharide monomer groups and amino acid groups associated with anammox consortia. Blue – Nitrogen, baseball – Cd, red – Oxygen, grey – C, circle - H. (For interpretation of the references to color in this figure legend, the reader is referred to the Web version of this article.)

Table 3
A literature compilation of calculated proton binding constants (pKa) and surface site concentrations of various natural consortia and the ability to adsorb Cd(II).

Living condition	pKa distribution	Site density/mmol g^{-1}	Adsorbed Cd/mol l^{-1}	Reference
Bacteria mixtures	5.0, 7.2, 9.7	4.50[a]	6.35×10^{-5}	Yee and Fein (2001)
Industrial contaminated	3.30, 4.77, 6.60, 9.05	0.30[b]		Borrok et al. (2004a)
Uncontaminated natural	3.12, 4.70, 6.57, 8.99	0.21[b]		Borrok et al. (2004b)
River	2.97, 4.73, 6.43, 9.18	0.38[b]	$(6.90–8.46) \times 10^{-5}$	Johnson et al. (2007)
Forest	3.30, 4.77, 6.59, 9.21	0.40[b]	$(4.63–6.23) \times 10^{-5}$	Johnson et al. (2007)
Crop	3.23, 4.81, 6.64, 9.22	0.38[b]	$(6.67–8.45) \times 10^{-5}$	Johnson et al. (2007)
Activated sludge	2.7-3.2,4.9-5.4, 6.1–7.2, 9.2–10	0.002[b]		Laurent et al. (2009)
Cyanobacteria	5.42,7.42, 9.95	33.4 ± 0.6[a]	7.81×10^{-6}	Liu et al. (2015)
Anaerobic Fe(II) oxidizing	4.83,6.21, 7.74, 9.28	2.75	0.21 μmol/mg	Martinez et al. (2016)
Anammox consortia	3.92, 6.69, 9.31	3.83[a]	7.12×10^{-6}	This study

[a] Site concentrations in mmol per dry mass.
[b] Site concentrations in mmol per wet mass.

weight of 10:1, and 70% of biomass were anammox consortia) of Cd to their cell surface. This is, of course, a variable amount because (1) we did not take into account competitive binding when other metals are available in solution in nature, (2) a fraction of the total Cd would be expected to complexed by dissolved organic ligands (Byrne et al., 1988), and (3) some fraction of Cd would be expected to precipitate as cadmium carbonate solids, as was observed in our Cd precipitation control experiments (Fig. 5). However, this study clearly demonstrates that planktonic anammox consortia are highly reactive and thus capable of accumulating trace metals from solution.

Previous research also demonstrates that anammox consortia produces more EPS as compared to activated sludge (Hou et al., 2015; Zhang et al., 2015b). It has been found that the electronegative groups of EPS, such as carboxyl and hydroxyl in polysaccharides, dominate bacterial aggregation through cation bridging interaction (Yuan et al., 2011), and these numerous binding sites ensured the formation of large flocs and aggregates. Hou et al. (2015) showed the forms of C-(C/H) (carbon chain and hydrocarbyl) accounted for 64.4% of the total C forms served as the main EPS component, comprising the hydrophobic component of the EPS. This observation once again strongly confirms the considerable hydrophobic component that exists in anammox consortia EPS, promoting bacterial aggregation. Furthermore, the elevated aggregation ability of anammox consortia increases the size of the particles to be separated, which remove trace metals together with settleable solids from raw wastewater.

When wastewater treatment is performed with the activated sludge process, the quality of the effluent is highly dependent on the efficiency of the solid-liquid separation processes (Sponza, 2003). Aggregation of macromolecules and small flocs can lead to a low turbidity of the effluent. In addition, macromolecular crowding can increase the robustness of gene expression, indicating that bacterial aggregation could increase the tolerance of bacteria to environmental inhibition by, for example, heavy metals (Tan et al., 2013; Hou et al., 2015). Such behavior is helpful to overcoming the susceptibility of anammox consortia to metal toxicity when they are applied for wastewater treatment.

In the near future, anammox consortia and anammox activity may be applied at large scales as the technology develops. Thus, our results are important in designing functionalized anammox processes for the preconcentration and removal of trace heavy metals together with N in wastewater treatment. This type of bioremediation process is especially efficient in the common case where wastewater with low to medium metal concentrations is to be treated. Treatment of wastewater with high metal concentrations can lead to rapid exhaustion, or even activity inhibition of biosorbent material, and thus a pre-treatment using other techniques, such as chemical precipitation (which is currently used for 90% of heavy metal removal from industrial wastewater) or electrolytic recovery before anammox technique, may be more effective and economical.

Our discussion has been focused on how anammox consortia bind significant concentrations of metals, using Cd(II) as a proxy for divalent metals, and may ultimately an important contributor to metal cycling in wastewater. Future efforts should be directed at experimentally determining the competitive adsorption of wastewaters containing several trace metals onto anammox consortia, along with assessing the impact of these metals on nitrogen removal efficiency in wastewater treatment processes.

5. Conclusions

Anammox consortia are highly reactive, due to the negatively-charged carboxyl and hydroxyl sites and positively charged amine sites. Carboxyl groups and hydroxyl groups associated with amino acids and polysaccharides, readily form stable complexes with Cd. The results highlight the potential role of anammox consortia in adsorbing metal cations in wastewater treatment systems. The electronegative carboxyl and hydroxyl sites additionally promotes bacterial aggregation due to their bridging ability. Facile bacterial aggregation and the reduction of toxicity due to macromolecular crowding suggest anammox consortia as a promising novel tool for the detoxification and cycling of metal cations in wastewater treatment streams.

Acknowledgements

The authors are grateful to the National Natural Science Foundation of China (No. 51578006) and Natural Science Foundation of Qinghai Science & Technology Department in China (No.2018-ZJ-910) to Zhao H.Z., China Postdoctoral Science Foundation (No. 2017M610708) and the Fundamental Research Funds for the Central Universities (ZX20180412) to Liu Y.X. for financial support. Alessi D.S. and Konhauser K.O. are funded by the Natural Sciences and Engineering Research Council of Canada (NSERC).

Appendix A. Supplementary data

Supplementary data to this article can be found online at

https://doi.org/10.1016/j.chemosphere.2019.01.025.

References

APHA, 1998. Standard Mentods for the Examination of Water and Wastewater. American Public Health Association.

Baes, C.F., Mesmer, R.E., 1976. Hydrolysis of Cations. Wiley Interscience Publication, New York.

Baun, D.L., Christensen, T.H., 2004. Speciation of heavy metals in landfill leachate: a review. Waste Manag. Res. 22 (1), 3–23.

Bi, Z., Qiao, S., Zhou, J.T., Tang, X., Cheng, Y.J., 2014. Inhibition and recovery of anammox biomass subjected to short-term exposure of Cd, Ag, Hg and Pb. Chem. Eng. J. 244, 89–96.

Borrok, D., Fein, J.B., Kulpa, C.F., 2004a. Proton and Cd adsorption onto natural bacterial consortia: testing universal adsorption behavior. Geochem. Cosmochim. Acta 68 (15), 3231–3238.

Borrok, D.M., Fein, J.B., Kulpa, C.F., 2004b. Cd and proton adsorption onto bacterial consortia grown from industrial wastes and contaminated geologic settings. Environ. Sci. Technol. 38 (21), 5656–5664.

Byrne, R.H., Kump, L., Cantrell, K., 1988. The influence of temperature and pH on trace metal speciation in seawater. Mar. Chem. 25 (2), 163–181.

Chen, H.H., Liu, S.T., Yang, F.L., Xue, Y., Wang, T., 2009. The development of simultaneous partial nitrification, anammox and denitrification (SNAD) process in a single reactor for nitrogen removal. Bioresour. Technol. 100 (4), 1548–1554.

Egli, K., Fanger, U., Alvarez, P.J.J., Siegrist, H., van der Meer, J.R., Zehnder, A.J.B., 2001. Enrichment and characterization of an anammox bacterium from a rotating biological contactor treating ammonium-rich leachate. Arch. Microbiol. 175 (3), 198–207.

Fein, J.B., Boily, J.-F., Yee, N., Gorman-Lewis, D., Turner, B.F., 2005. Potentiometric titrations of *Bacillus subtilis* cells to low pH and a comparison of modeling approaches. Geochem. Cosmochim. Acta 69 (5), 1123–1132.

Felten, J., Hall, H., Jaumot, J., Tauler, R., de Juan, A., Gorzsas, A., 2015. Vibrational spectroscopic image analysis of biological material using multivariate curve resolution-alternating least squares (MCR-ALS). Nat. Protoc. 10, 217–240.

Frisch, M.J., Trucks, G.W., Schlegel, H.B., Scuseria, G.E., Robb, M.A., Cheeseman, J.R., 2013. In: Gaussian, I.W.C. (Ed.), Gaussian 09, Revision d.01.

Herbelin, A.L., Westall, J.C., 1999. FITEQL 4.0: A Computer Program for Determination of Chemical Eqilibrium Constants from Experimental Data.

Hou, X.L., Liu, S.T., Zhang, Z.T., 2015. Role of extracellular polymeric substance in determining the high aggregation ability of anammox sludge. Water Res. 75, 51–62.

Jaeschke, A., Camp, H.J.M.o.d., Harhangi, H.R., Klimiuk, A., Hopmans, E.C., Jetten, M.S., Schouten, S., Sinninghe Damste, J.S., 2009. 16s rrna gene and lipid biomarker evidence for anaerobic ammonium-oxidizing bacteria (anammox) in California and Nevada hot springs. FEMS (Fed. Eur. Microbiol. Soc.) Microbiol. Ecol. 67 (3), 343–350.

Jiang, W., Saxena, A., Song, B., Ward, B.B., Beveridge, T.J., Myneni, S.C., 2004. Elucidation of functional groups on gram-positive and gram-negative bacterial surfaces using infrared spectroscopy. Langmuir 20 (26), 11433–11442.

Johnson, K., Szymanowski, J., Borrok, D., Huynh, T., Fein, J., 2007. Proton and metal adsorption onto bacterial consortia: stability constants for metal–bacterial surface complexes. Chem. Geol. 239 (1–2), 13–26.

Kimura, Y., Isaka, K., 2014. Evaluation of inhibitory effects of heavy metals on anaerobic ammonium oxidation (anammox) by continuous feeding tests. Appl. Microbiol. Biotechnol. 98 (16), 6965–6972.

Konhauser, K.O., 2007. Introduction to Geomicrobiology. Blackwell Publishing, Oxford.

Kumar, C.G., Joo, H.-S., Choi, J.-W., Koo, Y.-M., Chang, C.-S., 2004. Purification and characterization of an extracellular polysaccharide from haloalkalophilic bacillus sp. I-450. Enzym. Microb. Technol. 34 (7), 673–681.

Kuypers, M.M.M., Sliekers, O., Lavik, G., Schmid, M., Jørgensen, B.B., Kuenen, J.G., Strous, M., Jetten, M.S.M., Sinninghe Damsté, J.S., 2003. Anaerobic ammonium oxidation by anammox bacteria in the black sea. Nature 422 (6932), 608–611.

Lackner, S., Gilbert, E.M., Vlaeminck, S.E., Joss, A., Horn, H., van Loosdrecht, M.C.M., 2014. Full-scale partial nitritation/anammox experiences - an application survey. Water Res. 55, 292–303.

Laurent, J., Casellas, M., Pons, M.N., Dagot, C., 2009. Flocs surface functionality assessment of sonicated activated sludge in relation with physico-chemical properties. Ultrason. Sonochem. 16 (4), 488–494.

Li, H., Chen, S., Mu, B.Z., Gu, J.D., 2010. Molecular detection of anaerobic ammonium-oxidizing (anammox) bacteria in high-temperature petroleum reservoirs. Microb. Ecol. 60 (4), 771–783.

Liu, Y.X., Alessi, D.S., Owttrim, G.W., Petrash, D.A., Mloszewska, A.M., Lalonde, S.V., Martinez, R.E., Zhou, Q.X., Konhauser, K.O., 2015. Cell surface reactivity of *Synechococcus* sp. PCC 7002: implications for metal sorption from seawater. Geochem. Cosmochim. Acta 169, 30–44.

Lotti, T., Cordola, M., Kleerebezem, R., Caffaz, S., Lubello, C., van Loosdrecht, M.C.M., 2012. Inhibition effect of swine wastewater heavy metals and antibiotics on anammox activity. Water Sci. Technol. 66 (7), 1519–1526.

Marenich, A.V., Cramer, C.J., Truhlar, D.G., 2009. Universal solvation model based on solute electron density and on a continuum model of the solvent defined by the bulk dielectric constant and atomic surface tensions. J. Phys. Chem. B 113 (18), 6378–6396.

Martell, A.E., Smith, R.M., 1977. Critical Stability Constants, III. Other Organic Ligands. Plenum Press, New York.

Martinez, R.E., Konhauser, K.O., Paunova, N., Wu, W., Alessi, D.S., Kappler, A., 2016. Surface reactivity of the anaerobic phototrophic Fe(II)-oxidizing bacterium rhodovulum iodosum: implications for trace metal budgets in ancient oceans and banded iron formations. Chem. Geol. 442, 113–120.

Mulder, A., van de Graaf, A.A., Robertson, L.A., Kuenen, J.G., 1995. Anaerobic ammonium oxidation discovered in a denitrifying fluidized bed reactor. FEMS (Fed. Eur. Microbiol. Soc.) Microbiol. Ecol. 16 (3), 177–183.

Rich, J.J., Dale, O.R., Song, B., Ward, B.B., 2008. Anaerobic ammonium oxidation (anammox) in chesapeake bay sediments. Microb. Ecol. 55 (2), 311–320.

Schmitt, J., Flemming, H.-C., 1998. FTIR-spectroscopy in microbial and material analysis. Int. Biodeterior. Biodegrad. 41 (1), 1–11.

Sponza, D.T., 2003. Investigation of extracellular polymer substances (EPS) and physicochemical properties of different activated sludge flocs under steady-state conditions. Enzym. Microb. Technol. 32 (3), 375–385.

Stipp, S.L., Parks, G.A., Nordstrom, D.K., Leckie, J.O., 1993. Solubility-product constant and thermodynamic properties for synthetic otavite, $CdCO_3$(s), and aqueous association constants for the Cd (II)-CO_2-H_2O system. Geochem. Cosmochim. Acta 57 (12), 2699–2713.

Strous, M., Heijnen, J.J., Kuenen, J.G., Jetten, M.S.M., 1998. The sequencing batch reactor as a powerful tool for the study of slowly growing anaerobic ammonium-oxidizing microorganisms. Appl. Microbiol. Biotechnol. 50 (5), 589–596.

Tan, C., Saurabh, S., Bruchez, M.P., Schwartz, R., Leduc, P., 2013. Molecular crowding shapes gene expression in synthetic cellular nanosystems. Nat. Nanotechnol. 8 (8), 602–608.

Tang, C.-J., Zheng, P., Wang, C.-H., Mahmood, Q., Zhang, L., Zhang, J.-Q., Chen, X.-G., Chen, J.-W., 2011. Performance of high-loaded ANAMMOX UASB reactors containing granular sludge. Water Res. 45 (1), 135–144.

van de Graaf, A.A., de Bruijn, P., Robertson, L.A., Jetten, M.S.M., Kuenen, J.G., 1996. Autotrophic growth of anaerobic ammonium-oxidizing micro-organisms in a fluidized bed reactor. Microbiology 142 (8), 2187–2196.

Wang, C., Hu, X., Chen, M.L., Wu, Y.H., 2005. Total concentrations and fractions of Cd, Cr, Pb, Cu, Ni and Zn in sewage sludge from municipal and industrial wastewater treatment plants. J. Hazard Mater. 119 (1), 245–249.

Wang, L.L., Wang, L.F., Ren, X.M., Ye, X.D., Li, W.W., Yuan, S.J., Sun, M., Sheng, G.P., Yu, H.Q., Wang, X.K., 2012. pH dependence of structure and surface properties of microbial EPS. Environ. Sci. Technol. 46 (2), 737–744.

Wang, Z.K., Choi, O., Seo, Y., 2013. Relative contribution of biomolecules in bacterial extracellular polymeric substances to disinfection byproduct formation. Environ. Sci. Technol. 47 (17), 9764–9773.

Wen, S.F., Xu, Y.Z., 2016. Fourier Transform Infrared Spectroscopy Analysis, third ed. Chemical Industry Press (in Chinese).

Westall, J.C., 1982. Fiteql: A Computer Program for Determination of Chemical Equilibrium Constants from Experimental Data. Department of Chemistry, Oregon State University.

Yee, N., Fein, J., 2001. Cd adsorption onto bacterial surfaces: a universal adsorption edge? Geochem. Cosmochim. Acta 65 (13), 2037–2042.

Yuan, S.J., Sun, M., Sheng, G.P., Li, Y., Li, W.W., Yao, R.S., Yu, H.Q., 2011. Identification of key constituents and structure of the extracellular polymeric substances excreted by bacillus megaterium tf10 for their flocculation capacity. Environ. Sci. Technol. 45 (3), 1152–1157.

Zhang, Q.Q., Zhang, Z.Z., Guo, Q., Chen, Q.Q., Jiang, X.Y., Jin, R.C., 2015a. Anaerobic ammonium-oxidizing bacteria gain antibiotic resistance during long-term acclimatization. Bioresour. Technol. 192, 756–764.

Zhang, X., Zhang, Z.Z., Deng, R., Cheng, Y.F., Zhou, Y.H., Buayi, X., Wang, H.Z., Jin, R.C., 2015b. Behavior and fate of copper ions in an anammox granular sludge reactor and strategies for remediation. J. Hazard Mater. 300, 838–846.

Zhang, Z.T., Liu, S.T., Miyoshi, T., Matsuyama, H., Ni, J.R., 2016a. Mitigated membrane fouling of anammox membrane bioreactor by microbiological immobilization. Bioresour. Technol. 201, 312–318.

Zhang, Z.Z., Zhang, Q.Q., Xu, J.J., Deng, R., Ji, Z.Q., Wu, Y.H., Jin, R.C., 2016b. Evaluation of the inhibitory effects of heavy metals on anammox activity: a batch test study. Bioresour. Technol. 200, 208–216.

Zhao, Y., Truhlar, D.G., 2008. The M06 suite of density functionals for main group thermochemistry, thermochemical kinetics, noncovalent interactions, excited states, and transition elements: two new functionals and systematic testing of four M06-class functionals and 12 other functionals. Theor. Chem. Acc. 120 (1), 215–241.

Zirino, A., Yamamoto, S., 1972. A pH-dependent model for the chemical speciation of copper, zinc, cadmium, and lead in seawater. Limnol. Oceanogr. 17 (5), 661–671.